Development and preliminary assessment of an optical wave gauge

Grégory S. Payne[1], Jean-Baptiste Richon[2], David Ingram[3] and Johannes Spinneken[4]

[1]Institute for Energy Systems, School of Engineering, University of Edinburgh,
King's Buildings, Mayfield Road
Edinburgh EH9 3JL, U.K.
E-mail: gregory.payne@ed.ac.uk

[2]Laser & Imaging Sciences Ltd,
27 Ratcliffe Terrace,
Edinburgh EH9 1SX, U.K.
E-mail: jb.richon@limscience.co.uk

[3]Institute for Energy Systems, School of Engineering, University of Edinburgh
E-mail: david.ingram@ed.ac.uk

[4]Department of Civil and Environmental Engineering
Imperial College London
London SW7 2AZ, U.K.
E-mail: j.spinneken06@imperial.ac.uk

Abstract

A description and preliminary results are presented for a non-intrusive optical wave gauge based on the principle of optical triangulation. In the proposed implementation, a LASER source beaming vertically downwards generates a spot of scattered light at the water surface. The spot is imaged by an off-axis video camera, and instantaneous wave height measurements are obtained by processing of the spot images. The spot position on the image is then transformed into a height value using a polynomial best-fit function established by an initial calibration. The gauge geometry is set to give a measurement range of 300 mm. The calibration method and apparatus are described. A detailed statistical analysis of the calibration results is presented both for the optical wave gauge and for a conductivity wave gauge used as a comparison. Dynamic measurements for regular waves of 25 mm and 50 mm amplitudes at 1 Hz are carried out with both probes. The resulting time series data are compared to a theoretical fifth order Stokes solution. While overall agreement is good for both types of probe, optical wave gauge data are found to provide a better fit to the theoretical solution, especially in the vicinity of wave crests.

Keywords: wave measurement, laser, optical, wave gauge

© Proceedings of the 8th European Wave and Tidal Energy Conference, Uppsala, Sweden, 2009

Nomenclature

h	=	measured height
H	=	wave height
k	=	wave number
p	=	pixel data
V	=	voltage
α	=	slope
$\hat{\alpha}$	=	slope estimate
β	=	intercept
$\hat{\beta}$	=	intercept estimate
ε	=	error
σ	=	standard deviation

Subscript

i	=	observation index

1 Introduction

Tank testing is a key stage of the development of wave energy converters. It allows the performance assessment of a design in an accessible, controlled and repeatable environment at only a small fraction of the cost of sea trials. When carrying out tank testing, models are subjected to wave fields that must be characterised accurately.

Standard wave height measurement gauges present a number of drawbacks: they are intrusive, consisting typically of two thin, parallel vertical metal rods partly immersed. The water height is derived from the conductivity between the rods which increases with the immersion of the rods. A meniscus tends to form on the rods at the air-water interface, leading to measurement errors which can be significant when measuring small waves [1]. This issue is compounded further if the wave gauge is in a horizontally moving frame of reference, e.g. a towing carriage. Finally, the calibration of this kind of gauges is not very stable and has to be repeated regularly (in [2] it is suggested twice a day).

Optical wave gauges in contrast tend to be non intrusive. Most of them rely in some ways on LASERs (Light Amplification by Stimulated Emission of Radiation).

One of the first applications of LASERs to characterise wave fields relied on the Light Detection and Ranging (LIDAR) technique. A typical LIDAR system consists of a LASER source and of a photo sensor. The system is located above the water surface with the LASER beaming vertically downwards. Some of the LASER light is scattered by the water surface and bounces back towards the source where it is collected by the photo sensor. The distance between the LIDAR system and the water surface is derived from the time taken by the LASER light to travel from the source to the water surface and back. LIDARs have often been used for field measurements over large areas by mounting them on planes [3] or satellites.

Another technique relying on LASERs to characterise wave fields consists in measuring wave slope by exploiting the difference in refraction index between air and water. A LASER source is located below the water surface and is beaming vertically upwards. As the beam reaches the air-water interface, it is deflected from vertical according to Snell's law. The deflection angle is a function of the water surface angle to the vertical and of the ratio of the water refraction index to that of air. The deflected beam is collected above the water surface by an aspheric lens which focuses it on a photo detector. The lens is designed in such a way that the distance of the resulting LASER spot on the photo detector plan to the optical axis is proportional to the beam angle of incidence onto the lens. This technique does not actually measure wave height but wave slope. It is mainly used for spectral analysis of small waves such as capillary waves [4]. Although this system does not directly interfere with the water surface where the slope is measured, it is still intrusive in that it requires the laser source to be located at some depth below the water surface.

The system presented in this paper measures wave elevation by optical triangulation. All components are located above water so the system is truly non intrusive.

2 Working principle

The LASER source is located above the water surface and beams vertically downwards, generating a spot of scattered light at the water surface and a line of scattered light below the water surface. The spot and the line are imaged by a digital camera with an off-axis line of sight and a fixed position relative to the laser source. The upper end of the line of scattered light and the spot correspond to the water surface. Their precise location on the camera images are derived by image processing and transformed into a height value using a polynomial best-fit function established by an initial calibration. This principle is illustrated in Fig. 1 where two side view sketches show the water elevation measurement technique at a wave trough (Fig. 1a) and at a wave crest (Fig. 1b). The right hand side part of each sketch represents the image seen by the camera. The position of the spot is at the lower end of the range for the wave trough (Fig. 1a) and at the upper end for the wave crest (Fig. 1b).

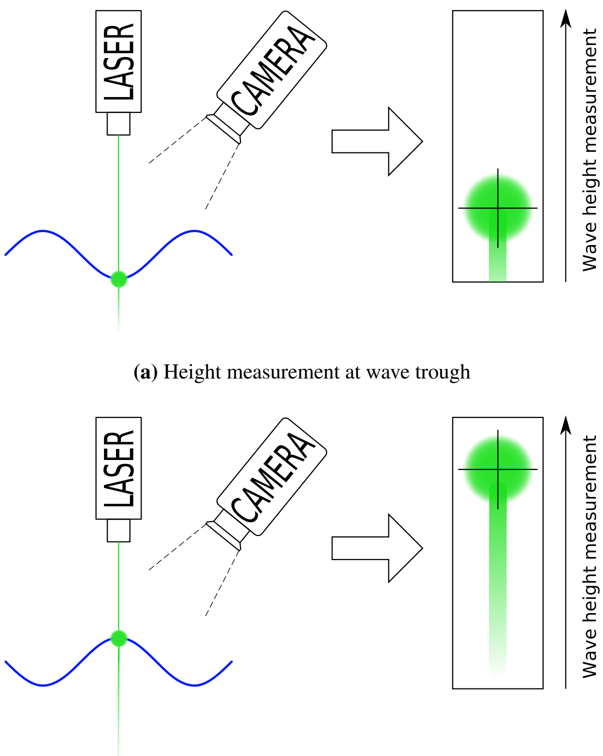

(a) Height measurement at wave trough

(b) Height measurement at wave crest

Figure 1: Optical wave gauge working principle

An optical wave gauge based on the same principle was developed in the early 80s [1]. A line array of 256 photodiodes was used in place of the camera. This gauge was used to study capillary waves with amplitudes of the order of 10 mm.

The system presented in this paper has a nominal range of 300 mm and uses a standard Charge-Coupled Device (CCD) camera with a VGA resolution (640×480 pixels). The range can be modified by the use of different camera lenses. Lenses with longer focal lengths will provide a shorter range but a finer resolution whereas lenses with shorter focal lengths will yield an increased range but at the expense of resolution. The LASER used is a 200 mW Diode Pumped Solid State (DPSS) LASER with a 532 nm wavelength. The calibration of this gauge is very stable in time as it only depends on the geometric parameters of the gauge set up. On the other hand external factors such as lighting and water surface quality must be minimised, as discussed in the next section.

Calibration is achieved by translating vertically the LASER-camera assembly above still water over a height corresponding to the range of the gauge. Images are acquired from the camera for a set of known vertical positions. Those images are used in combination with the height value at which they have been taken to derive the calibration curve of the gauge.

3 Image acquisition and processing

The image acquisition and processing sequences must ensure a reliable and accurate detection of the LASER spot on the free surface. On the recorded images the spot is always followed by a 'tail' of scattered light extending far below the water surface. The general principle underlying the detection of the spot and tail signals relies on statistical analysis of the grey-level pixel intensities along one or both axes of each image. An example image and the corresponding grey-level intensity profile are given in Fig. 2.

At the water surface, the appearance of the spot as seen by the camera will vary significantly with local wave slope, reflections caused by ambient lighting and contaminants that may be present at the point of impact of the beam, for instance solid particles or hydraulic oil. Probe settings are therefore adjusted so as to minimise any effects that these external factors may introduce in the measurements. The impact of ambient lighting can be largely removed by using a bandpass filter with a 532 nm centre wavelength, and by sampling only a narrow strip of image centered on the path followed by the LASER beam on the images during the measurements. To further reduce the impact of variations in the optical quality of the water surface on detection, the image exposure time is set to the shortest time still providing sufficient contrast in the image between the LASER beam path in the water and the dark background. The use of the shortest possible exposure time is also essential to minimise any time-averaging effects due to water motion occurring while the image is being recorded.

Two alternative image processing approaches were implemented to detect the LASER beam impact point on the water surface: one based on centroiding the spot image, the other based on grey-level threshold detection. Centroiding techniques offer a potential performance advantage over thresholding techniques since they inherently resolve the spot position to sub-pixel accuracy. In practice however, the spot shape and intensity profile were found to vary greatly in time; furthermore, in many cases the image of the beam intersection with the water surface looked much closer to a thick line with barely or no distinguishable spot feature at its extremity. In these cases, centroid detection actually tended to yield poorer results than threshold detection. Overall it was found that thresholding algorithms could be made to perform more consistently and over a broader range of operating conditions than their centroiding counterparts.

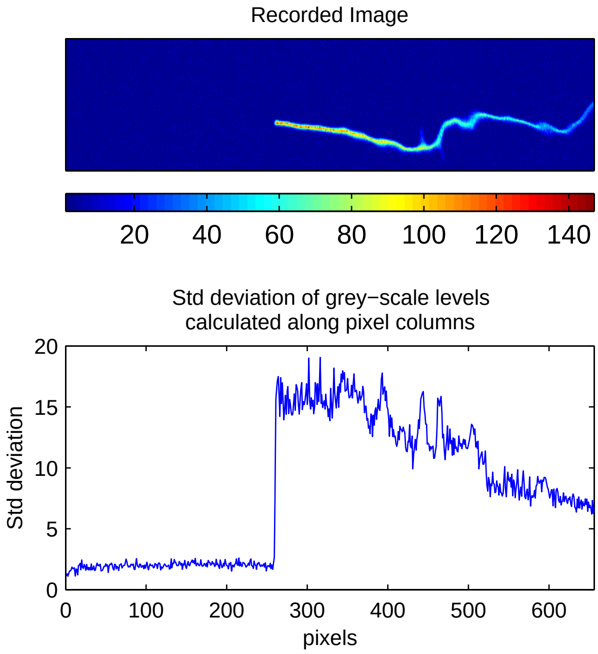

Figure 2: Image processing for the optical wave gauge. The camera image (top) shows the LASER trace in forced colours corresponding to grey-level intensities. The bottom graph shows the standard deviation of the grey-scale levels calculated along pixel columns for the image above. The x-axis pixel scale is the same for the graph and the image.

4 Calibration rig

The calibration rig is designed to be an integral part of the optical gauge itself. It can translate vertically the LASER-camera assembly over a 300 mm range. A picture of the rig is shown in Fig. 3.

The LASER and the camera are mounted on a 'translating beam' which is itself fastened to the moving block of a linear guide. The 'moving assembly' is driven up and down by a linear actuator. The actuator is fitted with a coarse digital motion encoder which allows position control with an accuracy of the order of 1 mm. To get more accurate height values, the rig is fitted with a digital scale unit whose absolute precision is 40 µm. The way the system is used for calibration is as follows. A target height is chosen. It is assigned to the control system of the linear actuator which relies on

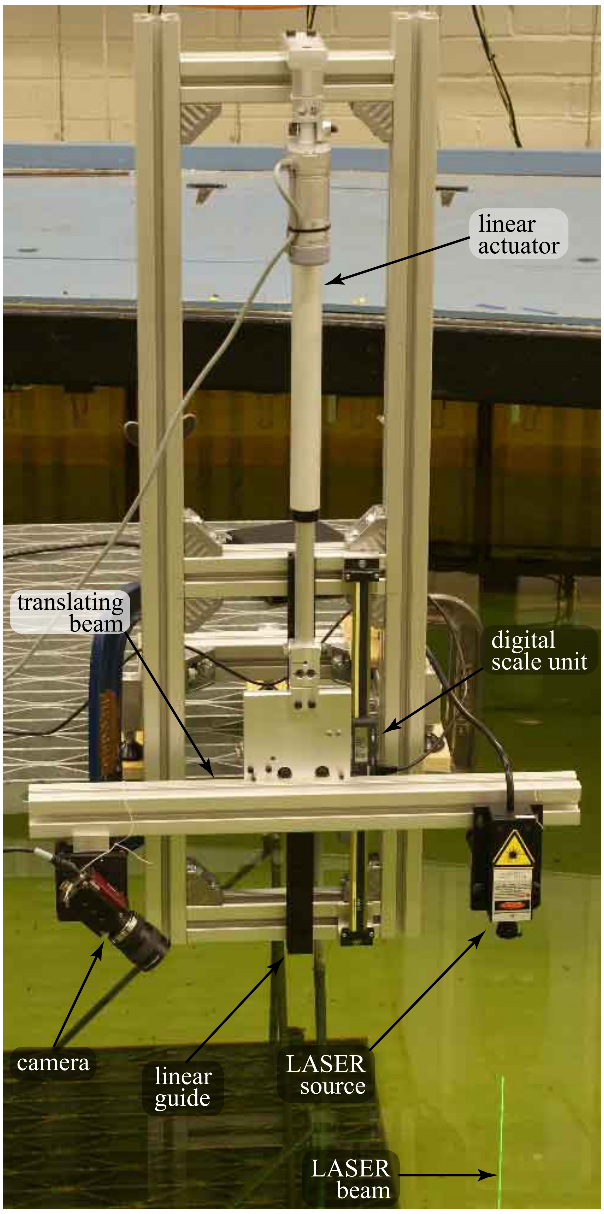

Figure 3: Optical wave gauge and calibration rig assembly set up in the Edinburgh curved tank. One can see the line of scattered light created by the LASER beam below the water surface.

the coarse encoder for its feedback loop. The moving assembly is driven to the target position with therefore a coarse accuracy. Once the actuator has stopped, a more accurate height value is read by the calibration system from the digital scale unit. The digital scale is not used in the control loop of the actuator.

The overall system is mounted on three levelling feet so that the orientation of the rail of the linear guide can be accurately set to vertical using a bulls eye spirit level.

5 Preliminary experimental results

To assess the performance of the optical wave gauge, static and dynamic tests have been carried out. The static test consists in the calibration of the gauge. Dynamic tests were carried out by comparing measurements from the optical wave gauge with that of a conductivity wave gauge in regular waves.

5.1 Wave gauge calibration

Calibration of both the optical and conductivity wave gauges was conducted over a 300 mm range. Eleven, uniformly distributed, target heights were used and each height was sampled four times. The calibration tests were then conducted in a randomised order to ensure that systematic errors were eliminated from the analysis. As explained in section 5, the height values reached were known with an accuracy of 40 µm. They were each time slightly different from their target value but within 1 mm of it. For both wave gauges the statistical package R [5] was used to perform a regression analysis and the residuals checked for heteroscedasticity by plotting the residuals against the observation number. The presence of a trend in the residuals when plotted in this way would indicate a systematic error in the measurements - and no such pattern was observed.

5.1.1 Conductivity wave gauge calibration

Initially the conductivity wave gauge measurements were fitted to the linear regression model

$$h_i = \beta + \alpha V_i + \varepsilon_i \qquad (1)$$

where h_i is the height of the i^{th} observation, V_i is the measured voltage at this height and ε_i is assumed to be a normally distributed error, $\varepsilon \sim N(0, \sigma^2)$. Using the method of least-squares, estimates of the slope $\hat{\alpha}$ and intercept $\hat{\beta}$ are then found. The errors are checked for heteroscedasticity by plotting the residuals against the height and normality by plotting a $Q-Q$ diagram against an assumed normal distribution.

Figure 4 shows the $Q-Q$ and residual plots. It can clearly be seen that although the linear fit leads to low residual values, the residuals are not normally distributed and there is evidence of a trend. Under such circumstances the idea of a linear fit must be rejected and a non-linear model sought.

Further investigation has shown that a cubic model:

$$h_i = \beta + \alpha_1 V_i + \alpha_2 V_i^2 + \alpha_3 V_i^3 + \varepsilon_i \qquad (2)$$

more fully explains the variation in the data, and shows no evidence of a trend in the residuals and also that the residuals, ε_i are normally distributed (see Fig 5). The resulting calibration curve is given by:

$$h_i \approx 150.3 + 31.92 V_i + 3.162 \times 10^{-2} V_i^2 + 4.063 \times 10^{-3} V_i^3 \qquad (3)$$

Although the coefficients of V_i^2 and V_i^3 are relatively small the analysis of variance test on the coefficients of the regression shows that they are all significant.

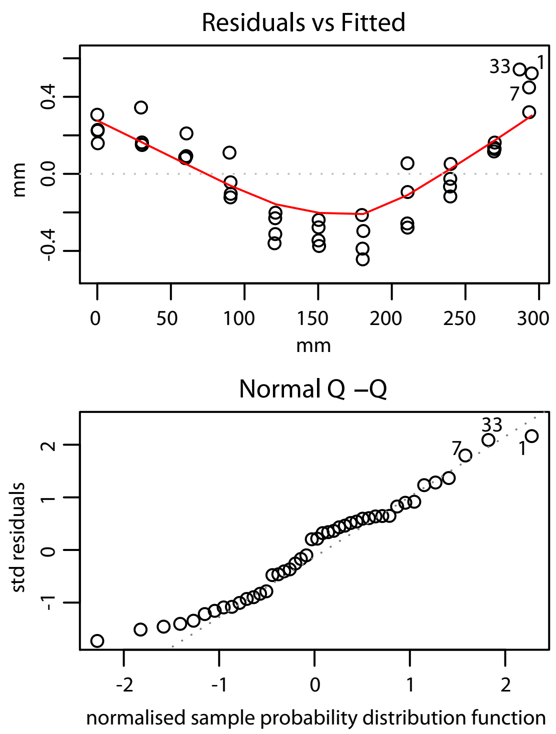

Figure 4: Residual and Normal Q-Q plot for the residuals from a linear regression model fitted to the observations from the conductivity wave gauge

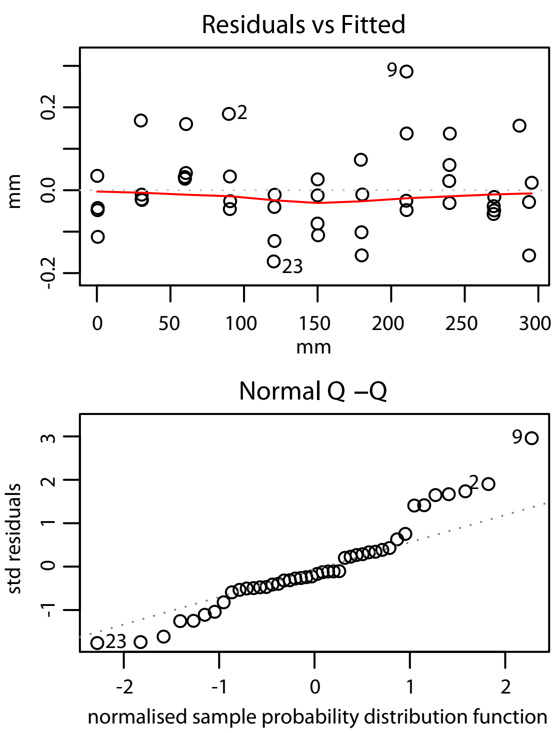

Figure 5: Residual and Normal Q-Q plot for the residuals from a cubic regression model fitted to the observations from the conductivity wave gauge

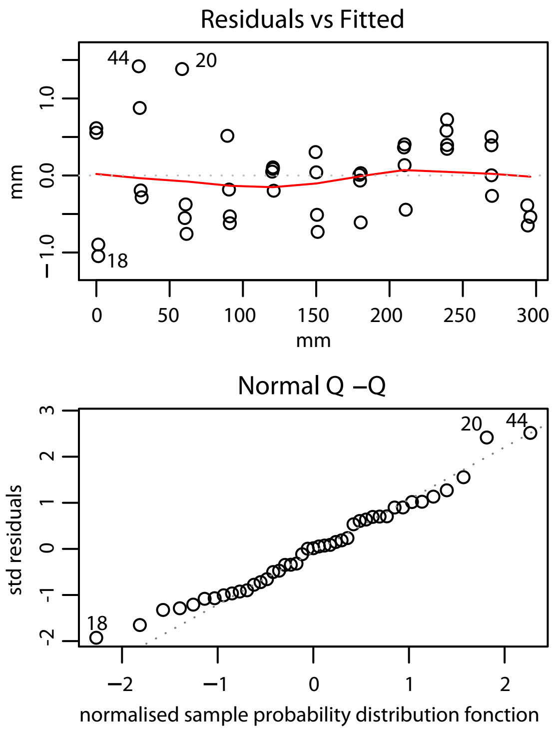

Figure 6: Residual and Normal Q-Q plot for the residuals from a cubic regression model fitted to the observations from the optical wave gauge

5.1.2 Optical wave gauge

As with the conductivity gauge a linear regression model does not fully explain the variation between the predicted height and pixel data from the optical wave gauge. Once again a cubic model has been found to be appropriate.

The analysis of variance shows that the quadratic coefficient is not significant and should be excluded from the regression. The resulting calibration curve equation is the following:

$$h_i \approx 298 - 0.3518 p_i - 2.821 \times 10^{-7} p_i^3 \qquad (4)$$

Fig. 6 shows the residual and normal $Q-Q$ plot for the fitted model, while Fig 7 shows the final calibration curve, together with the 95% confidence interval on the predicted height. Throughout the 300 mm range used for the calibration the 95% confidence interval is less than 1 mm wide and therefore difficult to distinguish from the calibration curve itself.

5.2 Dynamic tests

The tests were done in the University of Edinburgh curved tank [6]. Fig. 8 shows the experimental set up. The conductivity wave gauge can be seen in the bottom right corner of the picture. The line between the conductivity gauge and the LASER beam is parallel to the incoming wave fronts. The conductivity wave gauge was originally placed closer to the LASER beam (30 mm) in an attempt to get as similar wave conditions as possible at the two measurement points. It was however observed

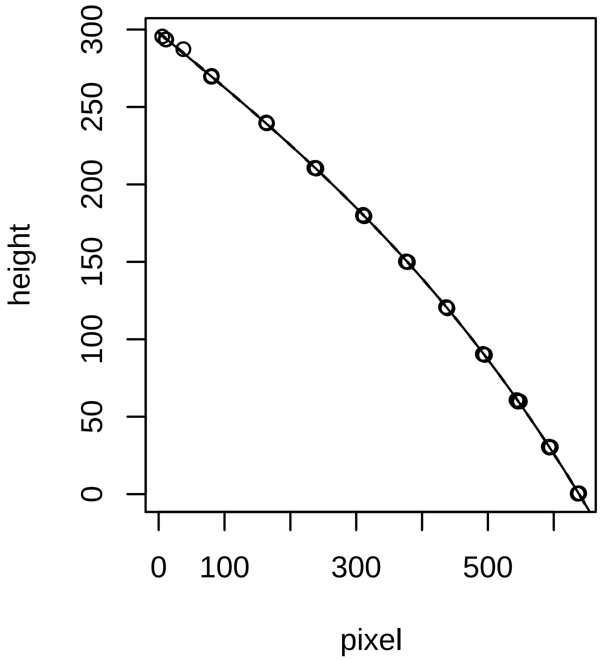

Figure 7: Calibration curve for the optical wave gauge, showing the observations from the calibration test (circles), the calibration curve (solid) and the 95% confidence intervals on the prediction (dashed).

that ripples were generated by the rods of the conductivity gauge. The ripples seemed to come from diffraction of the incoming waves by the rods but also from radiation. Waves were radiated when the menisci at the interface between the water surface and the rods flipped. This happens both at the wave crest and wave trough but more prominently at the wave crest. This is consistent with the fact that the wave profile is sharper at crest than at trough. It was decided to move the conductivity gauge further away from the LASER beam (210 mm) to minimise the effect of the ripples on the measurements from the optical wave gauge. The conductivity wave gauge was made of two 500 mm long stainless steel rods, 3 mm in diameter and 18 mm apart. A WG8 wave gauge box manufactured by Edinburgh Designs Ltd was used for signal conditioning.

Height measurements were carried out simultaneously with both gauges with regular waves of 1 Hz in frequency. Two nominal wave amplitudes were tested: 25 mm and 50 mm. For each test, signals from both wave gauges were sampled synchronously at 64 Hz for a duration of 3 s.

Figs. 9 and 10 show the time series for both wave amplitudes investigated. The signal from both gauges is compared with a fifth order Stokes theoretical solution [7]. Given the relatively deep water conditions (water depth of 1.2 m for 1 Hz waves) and the moderate steepness of the waves considered herein, this solution is regarded as an adequate reference. Deviation of the measured data from the theoretical solution is therefore considered to be due either to measurement inaccuracies or to spurious tank cross waves. It should be noted that the phase and height of the Stokes solution were adjusted to fit those of the gauge signals.

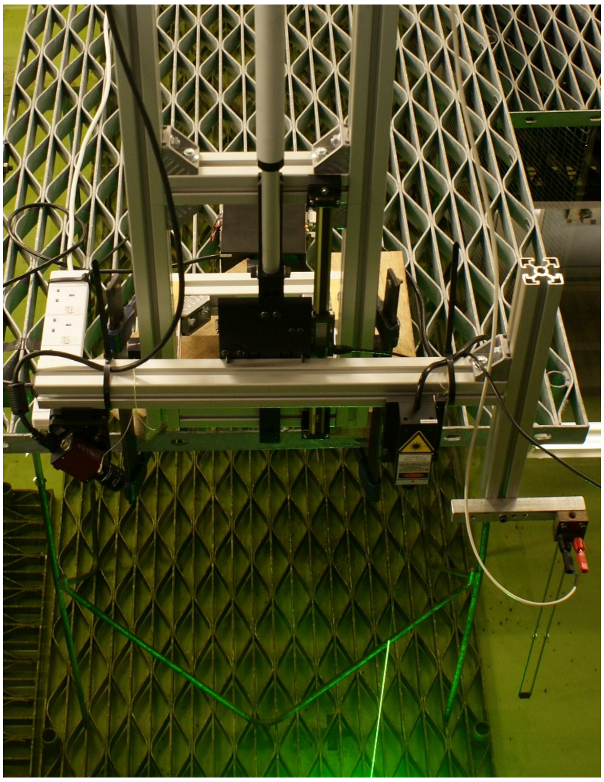

Figure 8: Optical wave gauge and conductivity wave gauge set up. The conductivity gauge can be seen in the bottom right corner.

The wave of Fig. 9 has a dimensionless wave steepness $Hk/2 \approx 0.1$. The data obtained using the optical wave gauge match very well the theoretical solution whereas some small deviations, in particular at the wave crest, remain when using the conductivity wave gauge. The discrepancies between the two measurement techniques are substantially more pronounced when considering the data shown in Fig. 10 where the steepness has been increased to $Hk/2 \approx 0.2$. The wave is now considerably steeper when compared to the previous test; evidence of its high non-linearity is clearly visible when observing the sharp crests and shallow troughs. Whilst the accuracy of both gauges is comparable in the vicinity of the troughs, the optical wave gauge yields a reading closer to theory at wave crests. The bottom plot of both figures shows that the optical wave gauge accounts better for the higher order wave components than the conductivity gauge.

6 Conclusions and further work

A non-contact optical wave gauge based on the principle of optical triangulation has been presented. Static calibration results using a precision digital scale unit as a reference indicate that this measurement technique

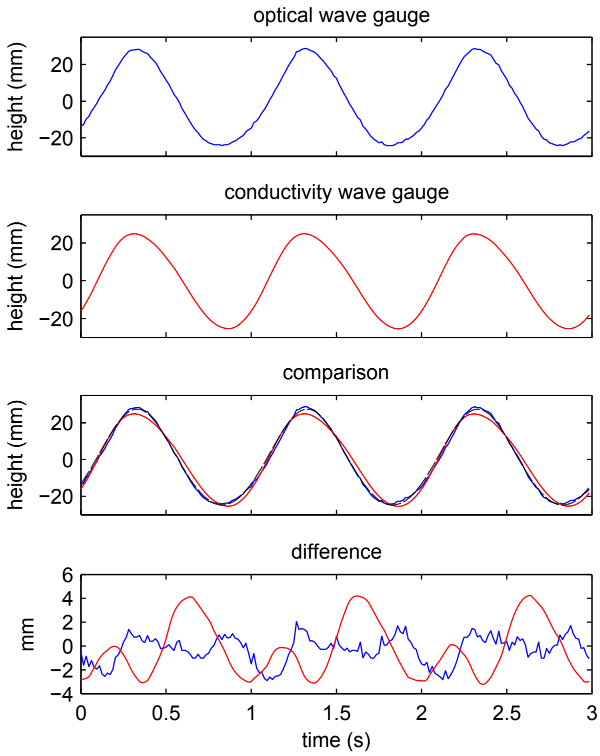

Figure 9: Optical (blue) and conductivity (red) wave gauges time series for 1 Hz, 25 mm amplitude waves. Starting from the top. The first plot corresponds to the optical wave gauge, the second to the conductivity wave gauge. The third plot compares the two gauge signals with a 5^{th} order Stokes model (dashed grey line). The forth plot shows each gauge time series minus the Stokes model time series.

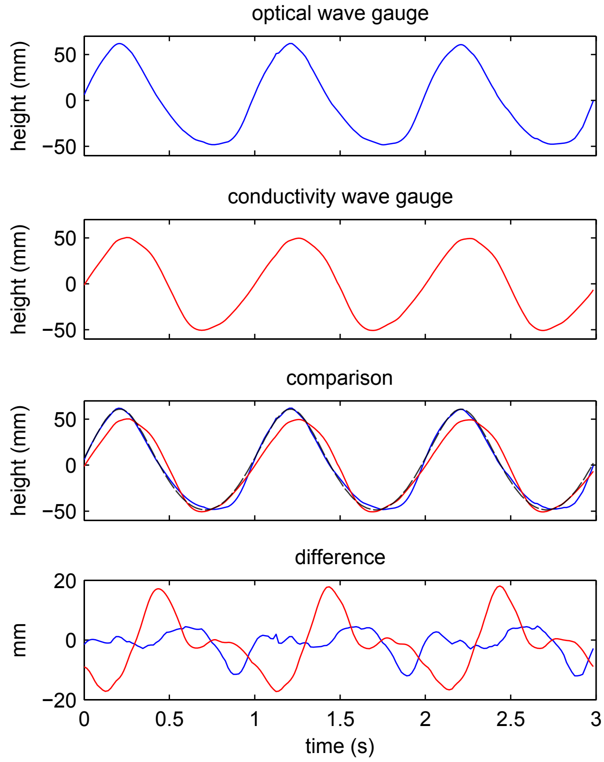

Figure 10: Optical (blue) and conductivity (red) wave gauges time series for 1 Hz, 50 mm amplitude waves. Starting from the top. The first plot corresponds to the optical wave gauge, the second to the conductivity wave gauge. The third plot compares the two gauge signals with a 5^{th} order Stokes model (dashed grey line). The forth plot shows each gauge time series minus the Stokes model time series.

is fit for purpose within the 300 mm range tested in the current configuration of the apparatus. Standard statistical analysis of the calibration data does not reveal any obvious measurement trend or bias. As expected it was found that the accuracy of the calibration is better in the central part of the measurement range. This is mainly due to camera lens aberrations, which are non-linear and much more pronounced near the edges of the field of view. When comparing this calibration to that of a conductivity wave gauge in the exact same conditions, performance is close although the conductivity gauge achieves smaller residuals against a third order polynomial model.

Dynamic time-series measurements with 1 Hz regular waves of 25 mm and 50 mm amplitude show that the optical wave gauge data produces good overall agreement with conductivity wave gauge data. Some of the visible differences may be attributable to the spatial inhomogeneity of the wave field generated in the Edinburgh curved tank. However, when comparing data sets from both gauges against a fifth order Stokes model, it was found that the optical wave gauge produces a noticeably closer fit to the model than the conductivity gauge. This is consistent with the tendency of intrusive rod and wire type wave gauges to filter out some of the higher order harmonic content [1]. It should be however noted that the diameter of the conductivity gauge rods used was possibly too large for the amplitude range of the waves measured.

As a preliminary conclusion it can be noted that the optical wave gauge performed well in the conditions of the tests. It offers an advantage over the conductivity gauge regarding the measurement of higher order wave components. Further experiments will be needed to confirm this point but it is an interesting prospect as accurate measurements of higher-order harmonic content is of importance in several research fields. These include wave dynamics but also wave-structure interaction where the second (or higher) harmonic present within the waves might excite a structural resonance.

The results obtained to date have shown that the detection of the LASER spot on the water surface can be made reliable. Further areas of work have been identified to improve the accuracy and the robustness of the measurements:

- Detailed analysis of the LASER beam profile in static conditions (no waves), from which a more precise thresholding criterion can be established for detecting the impact point of the beam on the water surface. This analysis will also provide useful information to determine whether detection accuracy would benefit from the use of a peak-fitting technique coupled to sub-pixel interpolation.

- Measurement of image background noise statistics during the calibration stage: for a fixed LASER power, the detection threshold could then be calibrated to a grey value that gives the closest matching results when compared to the reference gauge readouts.
- Inclusion in the image processing algorithm of a simple predictor centred on previous beam position to localise the current threshold search. This would make the algorithm near insensitive to spurious intensity peaks due to dust particles crossing the air path of the beam.
- Contrast optimisation across the images: the degree of focus of the LASER beam in the image depends on the position of the water surface relative to the camera lens and on the depth of field associated to the chosen lens aperture. This causes contrast variations across the image that result in poorer signal-to-noise ratios at the extremes of the measurement range. The extent to which this ultimately affects the measurements should be investigated for a range of camera lens adjustments and setups.

Acknowledgements

This work is supported by the UK Engineering and Physical Sciences Research Council through the SuperGen2 Marine Research Consortium. The third author wishes to acknowledge support for his position from the Scottish Funding Council and for their support of the Joint Research Institute in Energy with the Heriot-Watt University as a component part of the Edinburgh Research Partnership.

References

[1] H.-T. Liu, K.B. Katsaros, and M.A. Weissman. Dynamic response of thin-wire wave gauges. *Journal of Geophysical Research*, 87(C8):5686–5698, 1982.

[2] E. F. Thompson and C. E. Long. Wave measurement and analysis in laboratory flumes. In *IAHR Seminar on WAVE ANALYSIS AND GENERATION IN LABORATORY BASINS*, pages 75–90, Lausanne, Switzerland, September 1987.

[3] D.B. ROSS, V.J. CARDONE, and J.W. CONAWAY. Laser and Microwave Observations of Sea-Surface Condition for Fetch-Limited 17- to 25-m/s Winds. *IEEE Transactions on Geoscience Electronics*, GE-8(4):326 – 336, 1970.

[4] Robert J. Martinsen and Erik J. Bock. Optical measurements of ripples using a scanning-laser slope gauge: Part I - instrumentation and preliminary results. In *Proceedings of SPIE - The International Society for Optical Engineering*, volume 1749, pages 258–271, San Diego, CA, USA, July 1992.

[5] R Development Core Team. *R: A Language and Environment for Statistical Computing*. R Foundation for Statistical Computing, Vienna, Austria, 2008. ISBN 3-900051-07-0.

[6] J.R.M. Taylor, M. Rea, and D.J. Rogers. The Edinburgh curved tank. In *5^{th} European Wave Energy Conference*, pages 307–314, Cork, Ireland, September 2003.

[7] John D. Fenton. Fifth-order stokes theory for steady waves. *Journal of Waterway, Port, Coastal and Ocean Engineering*, 111(2):216 – 234, 1985.